MIT Open Access Articles

A multi-resolution ensemble study of a tropical urban environment and its interactions with the background regional atmosphere

Massachusetts Institute of Technology

A multi-resolution ensemble study of a tropical urban environment and its interactions with the background regional atmosphere

Xian-Xiang Li,[1] Tieh-Yong Koh,[2] Dara Entekhabi,[3] Matthias Roth,[4] Jagabandhu Panda,[2] and Leslie K Norford[5]

[1]   This study employed the Weather Research and Forecasting model with a single-layer urban canopy model to investigate the urban environment of a tropical city, Singapore. The coupled model was evaluated against available observational data from a sensor network and flux tower. The effects of land use type and anthropogenic heat (AH) on the thermal and wind environment were investigated with a series of sensitivity tests using an ensemble approach for low advection, high convective available potential energy, intermonsoon season cases. The diurnal cycle and spatial pattern of urban heat island (UHI) intensity and planetary boundary layer height were investigated. The mean UHI intensity peaked in the early morning at 2.2°C, reaching 2.4°C in industrial areas. Sea and land breezes developed during daytime and nighttime, respectively, with the former much stronger than the latter. The model predicted that sea breezes from different coastlines of the Malay Peninsula meet and converge, inducing strong updrafts. AH was found to play roles in all the processes studied, while the effect of different land use types was most pronounced during nighttime, and least visible near noon.

Citation: Li, X.-X., T.-Y. Koh, D. Entekhabi, M. Roth, J. Panda, and L. K. Norford (2013), A multi-resolution ensemble study of a tropical urban environment and its interactions with the background regional atmosphere, *J. Geophys. Res. Atmos.*, *118*, 9804–9818, doi:10.1002/jgrd.50795.

1. Introduction

[2]   Continuing urbanization is changing our environment in profound ways. One notable example is the canopy-layer urban heat island (UHI) effect, a result of microclimatic change caused by anthropogenic alterations to the Earth's surface [*Landsberg*, 1981]. The principal factors that generate UHI are the trapping of long-wave radiation during nighttime that takes place in the urban canopy, the thermal properties of the building materials, and the anthropogenic heat (AH) release due to human activities. Seasonal climatic conditions, daily synoptic conditions, and the diurnal cycle also play key roles in determining UHI character [*Arnfield*, 2003; *Oke*, 1982]. As a result, each urban area has a unique UHI particular to the circumstances found

there [*Yow*, 2007]. Urban environment and urban climate researchers have focused on UHI for decades. A comprehensive review of urban climate, including exchange of momentum, energy, and water, and the UHI can be found in *Arnfield* [2003]. *Grimmond* [2006] and *Souch and Grimmond* [2006] reviewed several large campaign-style urban climate studies. These studies revealed that the urban thermal conditions vary not only from those in rural surroundings but also within the urban area due to intra-urban differences in land use and surface characteristics.

[3]   The UHI during heat wave episodes (e.g., the 2003 summer heat wave in Europe) can pose a significant risk to human health or even life. Coastal, tropical, and rapidly growing cities are especially vulnerable to higher temperatures and impacts of urbanization [*Heisler and Brazel*, 2010]. Urbanization also has a long-term irreversible impact on decadal surface temperature trends. For example, rapid urbanization in China during 1978–2001 has resulted in a surface temperature increment of 0.05°C per decade [*Zhou et al.*, 2004]. More risks are expected as the sizes of urban areas grow continuously and the climate changes globally [*Hunt et al.*, 2013].

[4]   The urban areas also affect the structure and height of the planetary boundary layer (PBL), which is the lowest level of the atmosphere and directly interacts with the Earth's surface. Urban areas affect the PBL structure by modifying the surface roughness (resulting in more drag) and surface thermal conditions (usually hotter). An urban boundary layer thus forms, which is characterized by more

[1]CENSAM, Singapore-MIT Alliance for Research and Technology, Singapore.
[2]School of Physical and Mathematical Sciences, Nanyang Technological University, Singapore.
[3]Department of Civil and Environmental Engineering, Massachusetts Institute of Technology, Cambridge, Massachusetts, USA.
[4]Department of Geography, National University of Singapore, Singapore.
[5]Department of Architecture, Massachusetts Institute of Technology, Cambridge, Massachusetts, USA.

Corresponding author: X.-X. Li, CENSAM, Singapore-MIT Alliance for Research and Technology (SMART), 1 CREATE Way, #09-03 CREATE Tower, Singapore 138602, Singapore. (lixx@smart.mit.edu)

intensive turbulent exchange of momentum, heat, and moisture between the urban area and the overlying atmosphere.

[5] For many coastal cities, the sea/land breeze circulation also plays an important role in the local urban climate. This circulation can interact with the UHI and may have a mitigating effect on urban temperature extremes. For instance, the inland displacement and reduced magnitude of the Tokyo UHI in summer relative to winter is attributed to stronger summertime sea breezes [*Ichinose et al.*, 1999].

[6] The above physical processes in an urban environment may be modified by many factors. The maximum UHI intensity usually decreases with increasing wind speed and is most pronounced for clear skies. Local topography influences wind speed and direction, which can have a significant effect on urban boundary layer and the intensity and spatial structure of the UHI [*Yow*, 2007]. The UHI intensity varies seasonally and diurnally. Seasonal differences of UHI magnitude often result from seasonal variations in weather patterns. Some studies suggested a higher UHI intensity in summer than in winter [e.g., *Oke*, 1976; *Martin et al.*, 2000], while others suggested the reverse [e.g., *Souch and Grimmond*, 2006]. In the tropics, the greatest UHI intensity is usually achieved during dry seasons because of the higher nighttime cooling rates when rural areas are dry [*Jauregui*, 1997; *Roth*, 2007]. Diurnally, most studies suggest that the maximum UHI intensity is observed during nighttime [*Yow*, 2007].

[7] Many studies of the urban environment have been performed using numerical weather prediction (NWP) models such as the Pennsylvania State University/National Center for Atmospheric Research mesoscale model (known as MM5), the Weather Research and Forecasting (WRF) model or the UK Met Office Unified Model. With the dramatic development of computational capacity, NWP models can be run at horizontal resolutions of less than 1 km. It is therefore necessary to modify the physics of these models in order to account for the urban effects on evaporation rates, absorption, and reflection of solar radiation, storage of heat, and wind and turbulence fields. The common approach is to use urban canopy models (UCM) embedded within the NWP model. These schemes either model the urban canopy effects of streets and buildings using a single-layer [*Kusaka et al.*, 2001; *Kusaka and Kimura*, 2004] or multiple-layer parameterization [*Martilli et al.*, 2002].

[8] Sensitivity tests of UCMs [*Grimmond et al.*, 2011; *Lee et al.*, 2011; *Salamanca et al.*, 2011] show that more complicated models do not necessarily produce more benefits (e.g., more accurate details of the surface air temperature in urban areas). Using a mesoscale model with two different UCMs, *Holt and Pullen* [2007] studied the New York City area for 23 days. They found that both schemes are able to reproduce a UHI but underestimated its intensity. In addition, the sea breeze and inland penetration were also affected by the urban parameterizations (more so in the multiple-layer than the single-layer scheme). The performance of UCMs is highly sensitive to the urban parameters that define the urban morphology. This poses many challenges to the application of UCMs since many (at least 20) such urban parameters are needed, while their availability is currently limited to a few cities only [*Chen et al.*, 2011a]. A project called National Urban Database with Access Portal Tool [*Ching et al.*, 2009] was developed for the United States to produce gridded

fields of urban canopy parameters to improve urban meteorological simulations. It makes use of the availability of high-resolution urban building and land use data in various U.S. cities. Similar comprehensive efforts are, however, not evident outside the U.S.

[9] Various physical processes coexisting in urban areas are nonlinear, chaotic, and heterogeneous. Thus, any conclusions drawn from numerical simulations of a limited number of case studies may not be reliable or statistically significant. To overcome this problem, the ensemble approach has been employed in some studies. *Kusaka et al.* [2009] demonstrated that this approach can reduce uncertainties of conventional sensitivity experiments of a convective rainfall event over the Tokyo Metropolitan area surrounded by complex terrain. Using an ensemble approach, *Holt et al.* [2009] examined characteristics of sea breeze/heat island interactions and atmospheric transport and dispersion for Tokyo. More recently, *Inamura et al.* [2011] applied an ensemble approach to investigate the effects of urban areas on precipitation and wind systems during heavy rainfall in central Tokyo. Therefore, we employ the ensemble approach in this study.

[10] The majority of the previous studies on the urban environment and urban climate have been in the mid-latitudes [e.g., *Bohnenstengel et al.*, 2011; *Chemel and Sokhi*, 2012; *Pigeon et al.*, 2006]. However, much of the predicted urbanization and urban population growth will occur in (sub)tropical regions where UHIs negatively impact virtually all temperature-sensitive aspects of cities throughout the year [*Yow*, 2007]. The observational and numerical studies of a tropical coastal city, San Juan, Puerto Rico [*González et al.*, 2005; *Comarazamy et al.*, 2010; *Murphy et al.*, 2011], have highlighted the importance of urban climatology investigation in tropical regions under the condition of global climate change. This study will focus on a tropical city, Singapore, and will employ a single-layer UCM (SLUCM) coupled with WRF to parameterize the momentum and heat fluxes from urban areas. This approach is computationally relatively inexpensive and a practical means to improve simpler models [*Baklanov et al.*, 2009], which accounts for the urban area by parameterizing each grid's radiative and turbulence flux values and introducing a simple analytical wind profile formulation within the urban canopy. Several WRF/SLUCM studies have been carried out for various mid-latitude cities [*Chen et al.*, 2011b; *Lin et al.*, 2008; *Miao et al.*, 2009; *Salamanca et al.*, 2012], but few studies are available for tropical regions. The objectives of this study are to (1) evaluate the coupled WRF/SLUCM system's applicability to a tropical region, (2) investigate the diurnal cycle and spatial pattern of the UHI in a tropical city, and (3) study the impact of land use/land cover change and anthropogenic heat on the UHI, boundary layer development, and local circulations in a tropical city.

2. Model Configuration

2.1. The Study Area

[11] Singapore is an island state located between 1°09′N to 1°29′N and 103°36′E to 104°25′E. Its climate is a typical wet equatorial type (Köppen classification: *Af*) [*Essenwanger*, 2001] with uniformly high monthly mean
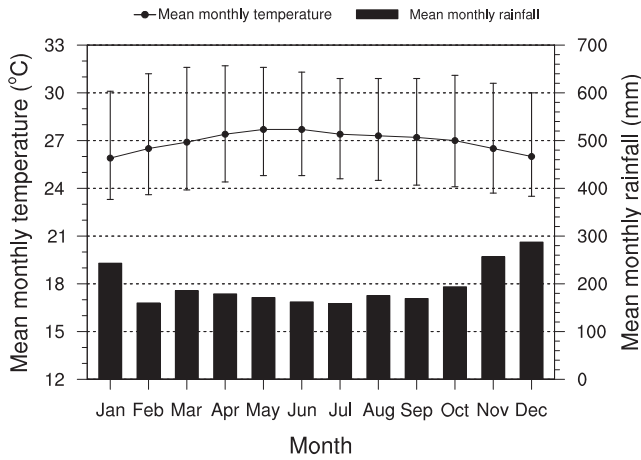
Figure 1. Singapore's general climatology based on the statistics of rainfall (from 1869 to 2011) and temperature (from 1929 to 2011) provided by Meteorological Service Singapore. Vertical bars represent the range between monthly average daily minimum and maximum temperatures.

temperature (26–27.7°C) and annual rainfall ($\approx$ 2300 mm) (see Figure 1). Singapore is located at the southern tip of the Malay Peninsula and is affected by East Asian monsoons. The northeast monsoon season from December to March, which is associated with the highest monthly rainfall and weaker winds, and the southwest monsoon season from June to September, which corresponds to a relatively drier period, are separated by two brief inter-monsoon or pre-monsoon periods [*Chia and Foong*, 1991]. There is no large and pronounced topography. The highest natural point is Bukit Timah at 164 m above sea level and is exceeded in height by the tallest buildings in the central business district (CBD). Ongoing land reclamation projects (mostly along the southern coastline) so far have increased the land area to the current 704 km^2.

[12] With a population reaching 5 million in 2011, Singapore has undergone rapid and dramatic urbanization during the past 45 years. The built-up area of Singapore increased from 28% in 1955 to 50% in 1998, while the farm area and forest decreased correspondingly [*Chow and Roth*, 2006]. Most of the urbanization is associated with the building of high-rise housing estates around the island and high-rise offices in the CBD in the south and industrial factories in the west. These significant changes of landscapes have profoundly affected the urban thermal environment [*Roth and Chow*, 2012].

2.2. The WRF Model

[13] In this study, the WRF model [*Skamarock et al.*, 2008] version 3.2.1 with Advanced Research WRF dynamics core developed by the National Center for Atmospheric Research is used to perform numerical simulations. The WRF model is a fully compressible, nonhydrostatic model with terrain-following mass coordinate system designed to simulate or predict regional weather and climate. The WRF model is applied to the 5 one-way nested domains shown in Figure 2a. The horizontal resolutions (grid sizes) of these five domains are 24.3 (76×76), 8.1 (79×91), 2.7 (112×112),

0.9 (112×112), and 0.3 km (211×130). In the vertical direction, there are 38 full sigma levels from the surface to 50 hPa, with the lowest 14 levels within the PBL to better resolve the PBL.

[14] Several physical parameterization schemes are employed in the coupling system to account for different physical processes involved. The Noah land surface model (LSM) provides surface sensible and latent heat fluxes and surface skin temperature as lower boundary conditions to WRF. It is based on a diurnally varying Penman potential evaporation approach, a multi-layer soil model, a modestly complex canopy resistance parameterization, surface hydrology, and frozen ground physics [*Chen and Dudhia*, 2001]. The Noah LSM can be coupled to various UCMs through the parameter urban fraction (F_{urb}) that represents the proportion of impervious surfaces in the WRF subgrid scale. For a given WRF grid cell, the Noah model calculates the temperature and surface fluxes for vegetated urban
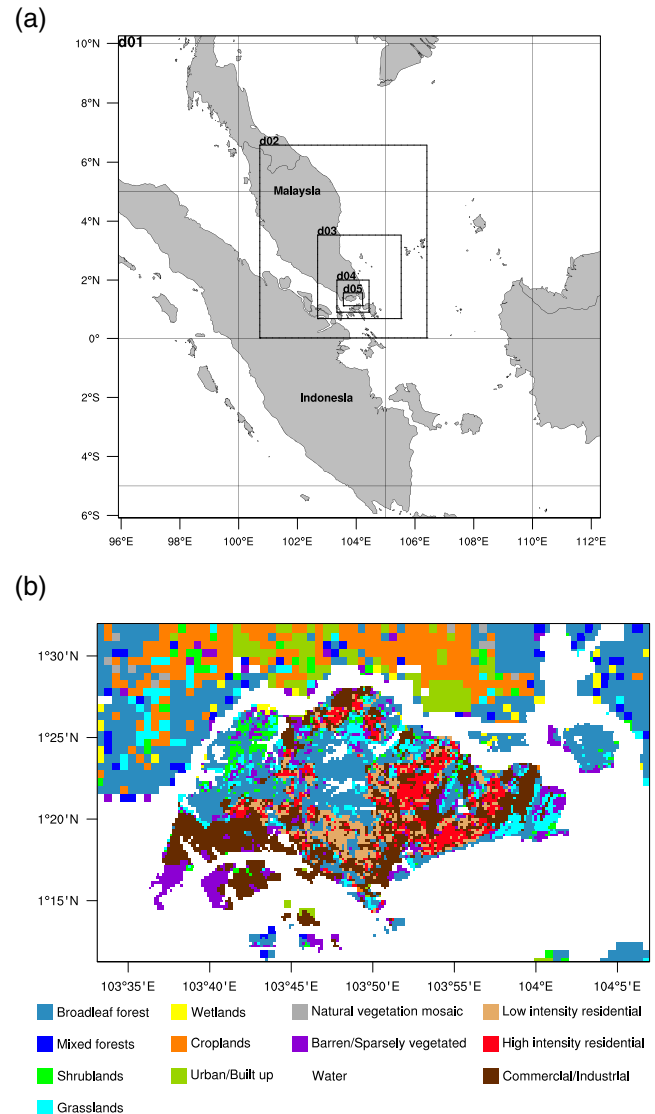
(a)

(b)

Figure 2. Configuration for WRF simulations. (a) The five nested domains and (b) the land use/land cover map for domain d05, which is centered on Singapore Island.

Table 1. Summary of Parameters Used in the Urban Canopy Model for Each Urban Land Use/Land Cover Type

Parameters	Commercial/Industrial	High Intensity	Low Intensity
Urban fraction	0.95	0.8	0.7
Mean building height (m)	15	15	8
Standard deviation of building height (m)	5	4	1
Roof width (m)	10	10	8
Road width (m)	8	8	5
Heat capacity of roof and wall (MJ m^{-3} K^{-1})	1.2	1.2	1.2
Heat capacity of road (MJ m^{-3} K^{-1})	1.6	1.6	1.6
Thermal conductivity of roof and wall (W m^{-1} K^{-1})	0.67	0.67	0.67
Thermal conductivity of road (W m^{-1} K^{-1})	1.0	1.0	1.0
Albedo of roof and wall	0.2	0.2	0.2
Albedo of road	0.1	0.1	0.1
Emissivity of roof and wall	0.9	0.9	0.9
Emissivity of road	0.95	0.95	0.95
Peak anthropogenic heat (W m^{-2}) (with diurnal profile in Figure 3)	113	18	13

areas (trees, parks, etc.) and the UCM provides the fluxes for impervious urban surfaces (buildings, roads, pavements, etc.). The total grid-scale sensible heat flux Q_H is then estimated as

$$Q_H = F_{veg} \times Q_{Hveg} + F_{urb} \times Q_{Hurb}, \qquad (1)$$

where Q_H is the total sensible heat flux from the surface to the WRF model lowest atmospheric layer, F_{veg} and F_{urb} are the fractional coverages of natural surfaces (e.g., grasslands, shrubs, crops, and trees in cities) and impervious surfaces (e.g., buildings, roads, and railways), respectively, Q_{Hveg} is the sensible heat flux from Noah for natural surfaces, and Q_{Hurb} is the sensible heat flux from UCM for impervious surfaces.

[15] The UCM coupled to the WRF/Noah system in this study is the SLUCM developed by *Kusaka et al.* [2001] and *Kusaka and Kimura* [2004]. This UCM has an intermediate level of complexity among the available UCMs for WRF. It assumes infinitely long street canyons parameterized to represent urban geometry but recognizes the three-dimensional nature of urban surfaces [*Chen et al.*, 2011a]. The SLUCM calculates the canyon drag coefficient and friction velocity using a similarity stability function for momentum. The total friction velocity is then aggregated from urban and nonurban surfaces and passed to WRF boundary layer schemes. Anthropogenic heat and its diurnal variation are taken into account by adding them to the sensible heat flux from the urban canopy layer. The SLUCM has about 20 parameters, most of which are listed in Table 1 along with their values prescribed in this study.

[16] Other physical parameterizations employed in this study are the following: Rapid Radiative Transfer Model long-wave radiation scheme, Dudhia short-wave radiation scheme, Mellor-Yamada-Janjić (MYJ) turbulence kinetic energy (TKE) PBL scheme, Monin-Obukhov surface layer scheme, Goddard microphysics scheme, and Kain-Fritsch cumulus scheme (for the three outer domains). The time integration step for d05 is 1 s, and the time step for the parent domain is 3 times that of the immediate child domain (i.e., the time step for domain d01 is 81 s).

[17] It has been reported that at high resolution (less than 1 km), WRF tends to produce some horizontal roll-type structures [e.g., *Miao et al.*, 2009; *Salamanca et al.*, 2012]. These structures are also observed in some of the

ensemble members simulated in this study (see section 2.4) during noon to early afternoon when the boundary layer is unstable. It is still debatable whether these roll structures are realistic or just numerical artifact [*Salamanca et al.*, 2012]. Unfortunately, no enough measurement data are available to help us in making any comment on this debate.

2.3. Input Data

[18] To represent the ever-growing urbanization of Singapore, up-to-date high-resolution land use/land cover data for Singapore have been obtained from Satellite Pour l'Observation de la Terre (SPOT) images and the Singapore Master Plan 2008 (Figure 2b). In accordance with the SLUCM's classification scheme, which restricts the urban land use/cover to three categories, the urban surface is further classified as high-intensity residential, low-intensity residential, and commercial/industrial areas. For regions outside Singapore, the MODIS 24-category land use/land cover data are used. The high-resolution topography data from Shuttle Radar Topography Mission (http://www2.jpl.nasa.gov/srtm/) are retrieved for the three inner domains. To test the effect of anthropogenic heat, a
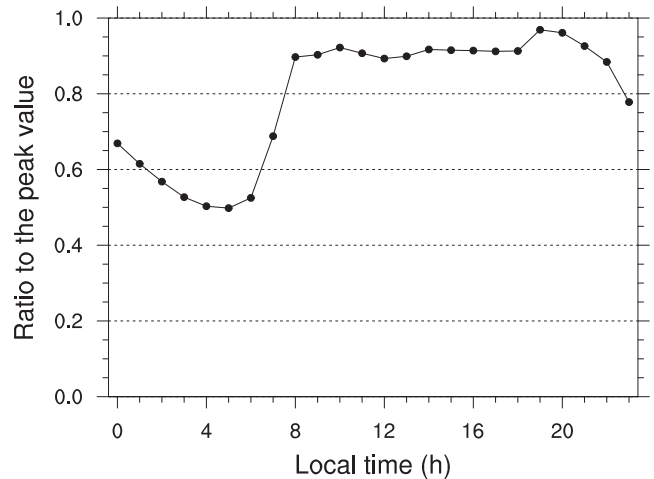

Figure 3. The diurnal profile of anthropogenic heat (the ratio to the peak value of each urban land use/land cover type) used in the SLUCM based on the data from *Quah and Roth* [2012]. The peak values are given in Table 1.
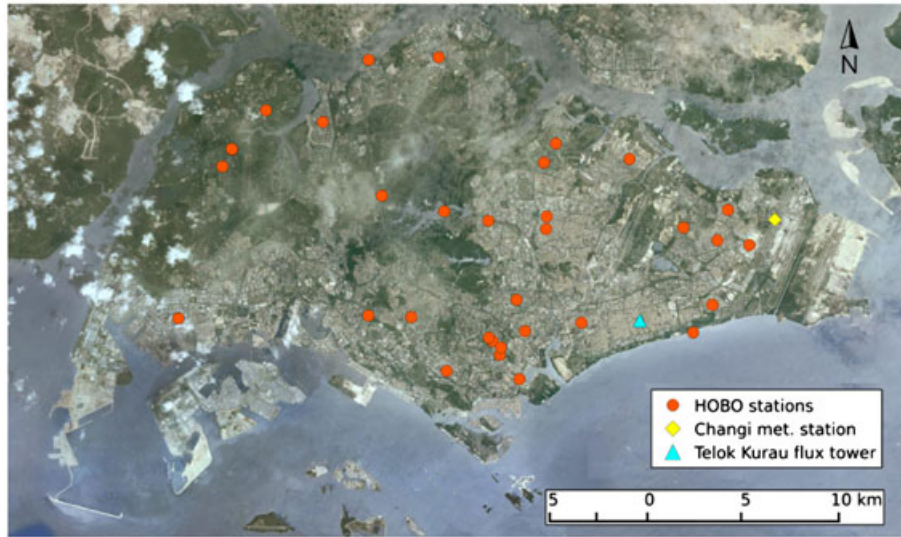
Figure 4. The observation network of HOBO sensors in Singapore for 2 m surface temperature and relative humidity (after *Li* [2013]). Also shown are the flux tower at Telok Kurau and the Changi meteorological station.

diurnally varying anthropogenic heat profile (Figure 3; the peak values are shown in Table 1) from *Quah and Roth* [2012] is utilized in the SLUCM.

[19] The initial and boundary conditions are taken from the NCEP's 6-hourly operational Global Final Analyses data at a $1.0° \times 1.0°$ resolution.

2.4. Ensemble Method

[20] To study the urban environment under nonlinear dynamics and with the coexistence of many environmental variables, we adopted the ensemble approach, in which simulations were carried out for a number of cases with similar synoptic conditions and the ensemble statistics were obtained from these simulations. To select the members of the ensemble, the weather conditions in Singapore from 2008 to 2009 were classified into eight categories based on (1) Convective Available Potential Energy (CAPE): high (> 1746 J kg^{-1}) or low (< 364 J kg^{-1}), (2) advection (the wind speed at 850 mb): high (> 7 m s^{-1}) or low (< 3 m s^{-1}), and (3) monsoon season: inter-monsoon or monsoon season. The classification is based on the statistics of the sounding record from the Changi meteorological station from 1990 to 2011. The criterion of high or low category is the 75 and 25 percentile of the wind speed and CAPE, respectively. The ensemble members are from the category of high CAPE, low

advection, and before southwest monsoon season. The intention for selecting this category is to minimize the effect of synoptic influences while maximizing the role of urban areas in the meteorological processes. A total of 28 members from April to May in 2008–2009 were selected to form the ensemble. All members are verified to belong to the high CAPE and low-advection category in WRF. Each member has a 36 h simulation time starting at 12 UTC (= LT − 8h) of the previous day and ending at 00 UTC of the next day. The first 12 h are treated as spin-up time and discarded when calculating the ensemble statistics.

3. Model Evaluation

[21] To validate the WRF/SLUCM system's capability in reproducing key characteristics of urban surface processes, we perform a model evaluation exercise using the temperature and humidity data from an urban-scale microclimate network (see Figure 4).

3.1. Surface Temperature and Humidity

[22] Shown in Tables 2 and 3 are the comparison of the simulated and observed 2 m surface temperature and specific humidity, respectively, during April–May 2008. According to the record of a meteorological station on the campus of

Table 2. Comparison of Simulated and Observed 2 m Surface Temperature (°C) for Different Land Use/Land Cover Types[a]

Land Use/Land Cover	N_stn (N_data)	Mean		Std dev		MB	RMSE	HR	IOA	α	ρ	η
		Obs	WRF	Obs	WRF							
Evergreen forest	3 (1371)	27.04	26.87	1.97	1.97	−0.17	1.62	0.82	0.81	0.33	0.67	1.00
Open shrublands	4 (1210)	25.87	26.52	2.48	2.22	0.65	1.73	0.79	0.86	0.23	0.77	1.00
Grasslands	1 (161)	26.90	27.31	2.06	2.05	0.4	1.48	0.88	0.86	0.24	0.76	1.00
Water	1 (118)	26.52	27.56	1.53	0.91	1.04	1.61	0.78	0.65	0.48	0.59	0.88
Low intensity	3 (1211)	27.61	26.82	2.16	2.20	−0.79	2.17	0.62	0.74	0.43	0.57	1.00
High intensity	9 (4320)	28.48	27.56	1.73	1.88	−0.92	1.68	0.79	0.78	0.30	0.70	1.00
Commercial/industrial	10 (4522)	27.93	28.04	1.95	1.88	0.11	1.55	0.83	0.82	0.33	0.67	1.00
Mean	31 (13438)	27.74	27.47	2.10	2.03	−0.27	1.68	0.79	0.82	0.32	0.68	1.00

[a]N_stn and N_data are number of observation stations and number of data points, respectively.

Table 3. Same as Table 2 but for 2 m Specific Humidity (g kg^{-1})

Land Use/Land Cover	N_stn (N_data)	Mean		Std dev		MB	RMSE	HR	IOA	α	ρ	η
		Obs	WRF	Obs	WRF							
Evergreen forest	3 (1147)	20.19	18.00	0.97	1.03	−2.18	2.57	0.44	0.34	0.93	0.07	1.00
Open shrublands	2 (579)	19.96	17.71	1.09	1.03	−2.24	2.71	0.49	0.36	1.03	−0.03	1.00
Grasslands	1 (161)	19.59	17.90	0.55	0.98	−1.69	2.01	0.66	0.27	0.96	0.05	0.86
Water	1 (118)	20.27	20.05	0.54	0.65	−0.22	0.91	0.97	0.31	1.09	−0.09	0.98
High intensity	7 (2986)	19.70	17.61	0.94	1.10	−2.09	2.46	0.46	0.36	0.82	0.18	0.99
Commercial/industrial	9 (3469)	19.86	17.57	1.06	1.16	−2.30	2.72	0.44	0.36	0.85	0.15	1.00
Mean	23 (8985)	19.86	17.68	1.00	1.15	−2.18	2.59	0.46	0.36	0.85	0.15	0.99

National University of Singapore, only a few brief rainfall events occurred during this period. The statistics of mean bias (MB), standard deviation, root-mean-square error (RMSE), hit rate (HR), and index of agreement (IOA) are calculated. The HR is defined as [*Schlünzen and Katzfey*, 2003]

$$H = \frac{1}{m} \times \sum_{i=1}^{m} n_i, \qquad (2)$$

where

$$n_i = \begin{cases} 1 & \text{for } |O_i - P_i| < A, \\ 0 & \text{for } |O_i - P_i| \geq A, \end{cases}$$

and m is the number of comparison values, O_i and P_i are observed and predicted results, and A is the desired accuracy. For surface temperature and specific humidity, this accuracy is 2°C and 2 g kg^{-1}, respectively, following *Cox et al.* [1998]. The HR is a reliable overall measure for describing model performance. It is able to consider the measurement uncertainty, which is much more difficult to evaluate using the bias or RMSE measures [*Schlünzen and Katzfey*, 2003]. The IOA is a measure of degree to which a model's predictions are error free and was proposed by *Willmott* [1981] as

$$d = 1 - \frac{\sum_{i=1}^{m}(P_i - O_i)^2}{\sum_{i=1}^{m}(|P_i - \overline{O}| + |O_i - \overline{O}|)^2}, \qquad (3)$$

where $\overline{O}$ is the average observation values. This dimensionless index has a theoretical range of 1.0 (for perfect agreement) to 0 (for no agreement).

[23] The overall 2 m temperature mean bias averaged over all the land uses is only –0.27°C, with a overall HR of 0.79 and IOA of 0.82. The lowest absolute mean bias (0.11) is observed for commercial/industrial land use type, with a HR of 0.83 and IOA of 0.82. However, the other two urban land use types (high- and low-intensity residential) show relatively higher absolute mean bias, which suggests that the UCM performs better for denser built-up areas, an observation in accordance with that of *Miao et al.* [2009].

[24] While the overall performance of the simulated 2 m surface temperature is good, the simulated 2 m specific humidity consistently underpredicts the observations (Table 3). The same underprediction was reported in *Miao et al.* [2009] for their case study of Beijing. It is possibly due to underprediction of the surface evaporation (and the associated latent heat flux) from the UCM discussed in the next subsection. Another possible reason in our case is due to the inherent problems of the HOBO sensor. When relative humidity reaches above 90%, which occurs frequently in Singapore, the HOBO sensor needs quite a long restoration

time from near saturation. The measurements subsequent to saturation are therefore usually higher than the real values [*Onset Computer Corporation*, 2007].

[25] To gain further insight into the model prediction errors, the normalized error variance diagnostic is introduced here [*Koh et al.*, 2012]:

$$\alpha = 1 - \rho\eta, \qquad (4)$$

where

$$\alpha = \frac{\sigma_D^2}{\sigma_O^2 + \sigma_P^2}, \qquad 0 \leq \alpha \leq 2; \qquad (5a)$$

$$\eta = \frac{\sigma_O \sigma_P}{\frac{1}{2}(\sigma_O^2 + \sigma_P^2)}, \qquad 0 \leq \eta \leq 1, \qquad (5b)$$

σ denotes standard deviation and D is the difference between prediction P and observation O. Here α is the normalized error variance [*Koh and Ng*, 2009], which was shown not to depend on observation variability (unlike the error variance itself), thus yielding insights into the model prediction errors in a mesoscale model. ρ is the correlation coefficient (a measure of phase error), and η is a measure called "variance similarity" (a measure of amplitude error). The variance similarity compares the standard deviation of the model prediction and observation, achieving a maximum value of 1 when the two are identical but tends to 0 monotonically when one of them becomes much larger than the other. The calculated α, ρ, and η for temperature and humidity are also listed in Tables 2 and 3, respectively. It is clear from equation (4) that the larger α (smaller accuracy) of surface temperature across different land use types is attributed to smaller ρ (larger phase error), while η is close to 1 (small amplitude error) for all land use types except water. For specific humidity, all α values are quite large and for some land use types, α values are even larger than 1, showing that the model has no prediction skill for specific humidity. (This is because a random forecast with no correlation with observation would have $\alpha = 1$, beating the performance of the model in these land use types). Similarly, the large α can also be attributed to poor (or even negative) correlation as seen in Table 3.

3.2. Surface Energy Balance

[26] The accurate prediction of surface energy balance is the fundamental requirement for the atmospheric model. The surface energy balance for urban area reads

$$Q^* + Q_F = Q_H + Q_E + \Delta Q_S, \qquad (6)$$

where Q^* is the net all-wave radiation, Q_H and Q_E are the turbulent sensible and latent heat fluxes, respectively, ΔQ_S is the net heat storage flux, and Q_F is the anthropogenic heat
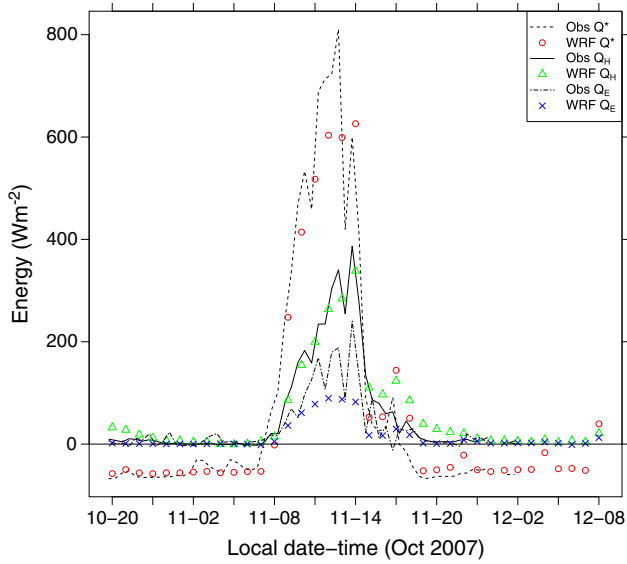
Figure 5. Comparison of observed and WRF-simulated energy balance components for the case of 10–12 October 2007. Note that the observational data are sometimes missing.

flux. The net heat storage includes the energy storage within the buildings, the road and underlying soil, and for some models, the air space within the street canyon [*Grimmond and Oke*, 1999]. Here the net heat advection is assumed to be negligible.

[27] Due to the limited availability of energy balance data and strict criteria for case selection (described in section 2.4), only one case study for the period 00 UTC 10 October to 00 UTC 12 October 2007 was selected for comparison. Given the low seasonal variability typical of the tropics and the fact that October is also within an inter-monsoon season, the present comparison should also be representative for the members of the ensemble. The energy balance data are from a flux tower in Telok Kurau (see Figure 4), which is located in a high-intensity residential neighborhood of eastern Singapore. The average building height is about 8.9 m within 500 m of the site. Figure 5 compares the observed and simulated energy balance components. It is evident that the WRF model correctly captures the diurnal cycle of Q^*, Q_H, and Q_E. However, the simulated Q^* fails to capture the peak value of about 800 Wm^{-2} observed at noon on 11 October 2007. It is noteworthy that the model is able to capture the sharp decrease in Q^* during the afternoon of 11 October 2007, due to light rain (recorded by a rain gage next to the flux tower). The simulated Q_H agrees very well with the measured values, with only a slight overprediction during the transition from day-time to nighttime in 11 October. The simulated Q_E agrees well with the measurement during the night when the values are small, but the model considerably underpredicts Q_E during the daytime. This is in line with simulated specific humidity lower than the observed values, as discussed in the previous section. *Grimmond et al.* [2010] concluded that the coupled WRF/SLUCM model has the best overall capability to model Q^* and least capability to model Q_E.

[28] Having demonstrated that the WRF/SLUCM model can reasonably well reproduce the surface energy balance

and surface temperature, the next sections will use the model to examine the diurnal variability of the UHI and the local circulation in Singapore.

4. Results and Discussions

[29] To examine the impact of urbanization on the local urban environment, three sensitivity tests are carried out for all the members in the selected ensemble (section 2.4). The first one is the control simulation with real land use and urban categories (hereafter referred to as CONTROL). The second is a simulation with the urban categories replaced
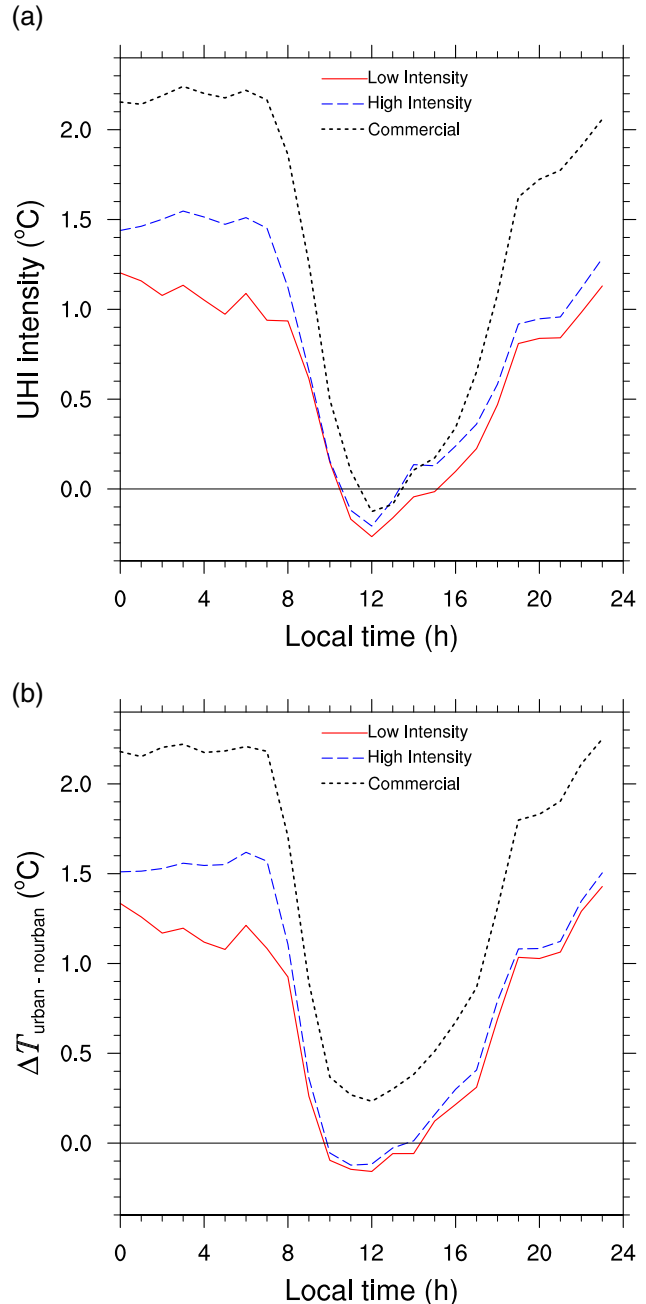
(a)

(b)

Figure 6. (a) Diurnal variation of UHI intensity for CON-TROL cases and (b) diurnal variation of urban increment (CONTROL cases minus NoURBAN cases).
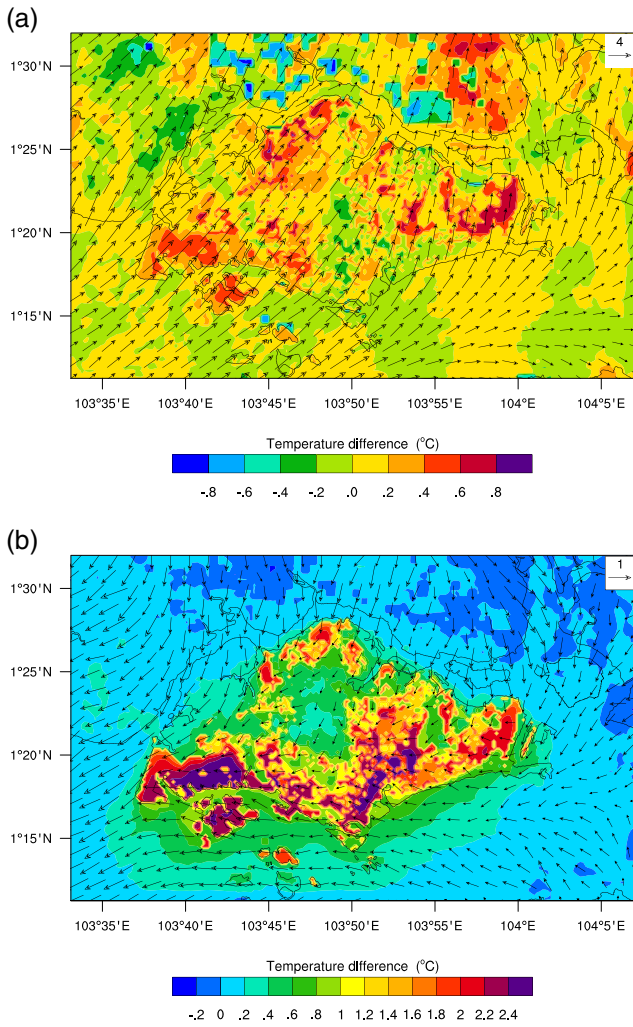
Figure 7. Difference in ensemble mean 2 m surface temperature of CONTROL and NoURBAN cases at (a) 14:00 LT and (b) 04:00 LT. The vector is the 10 m surface wind field of the CONTROL case at the same time (unit: m s^{-1}).

with rural (open shrub) land use/land cover type (hereafter referred to as NoURBAN). The last one is a test with real land use and urban categories, but the anthropogenic heat associated with urban areas is turned off (hereafter referred to as NoAH). The results presented in this section are for domain d05 unless otherwise specified. In all the UHI calculations, the rural reference is chosen as open shrubland, because we find the greatest temperature difference is usually observed during nighttime between commercial/industrial areas and open, vegetated areas (i.e., open shrubland), rather than the evergreen forest area. This is consistent with the findings by *Hawkins et al.* [2004] for Phoenix, Arizona and *Murphy et al.* [2011] for San Juan, Puerto Rico. The reason for these findings can be attributed to the large sky view factors in open areas, which enhance long-wave cooling after sunset.

4.1. UHI Pattern

[30] The UHI intensity due to urbanization can be calculated in two ways. The first way is the traditional one defined as the difference in the 2 m temperature between

urban and nearby undeveloped rural areas (open shrub land in this case). The second is the difference in the 2 m temperatures between the CONTROL and NoURBAN simulations, which is termed as "urban increment". This method largely removes such effects as sea breezes, impacts of clouds, or topography that might alter the surface temperatures [*Bohnenstengel et al.*, 2011].

[31] The diurnal variation of the ensemble UHI intensity calculated by these two methods (averaged over the same land use type in domain d05) is shown in Figures 6a and 6b, respectively. It can be seen that the UHI intensities resulted from these two methods are quite similar. Throughout much of the night, the ensemble UHI intensities of commercial/industrial and high-intensity residential areas are smooth, staying at their daily peak of 2.2°C and 1.5°C,
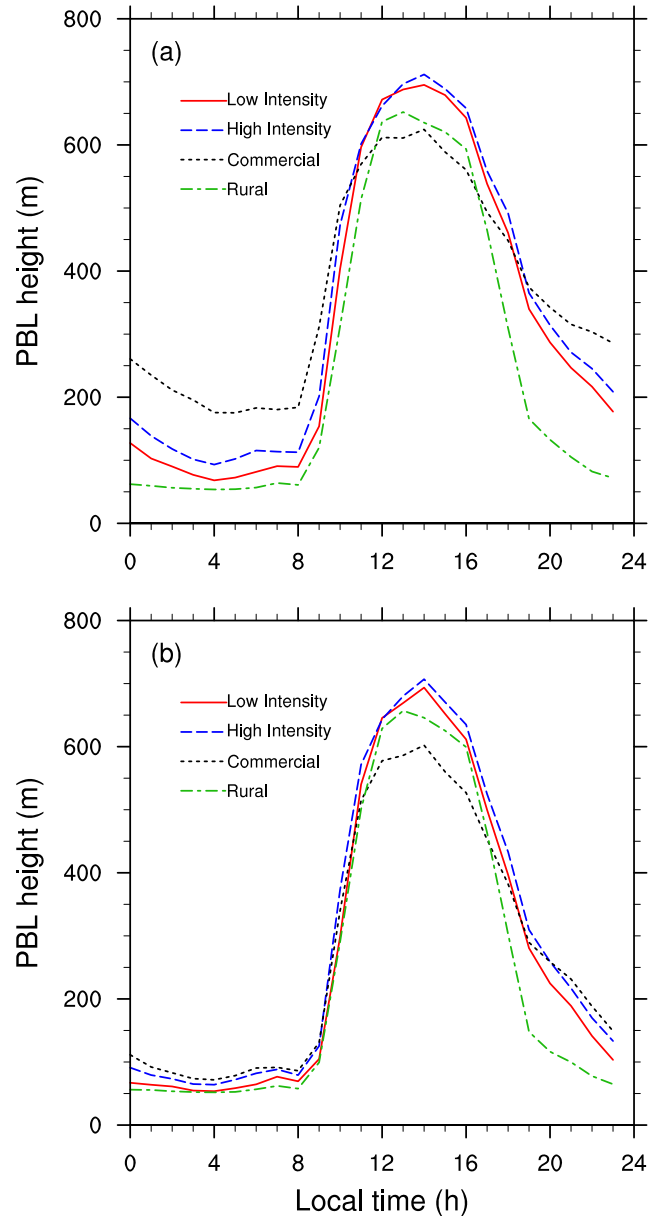

Figure 8. Diurnal variation of the ensemble mean PBL height averaged by land use/land cover types. (a) CONTROL case and (b) NoAH case.
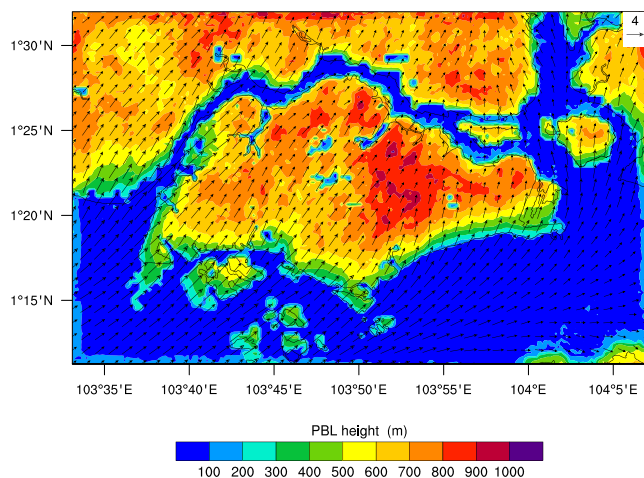
Figure 9. The ensemble mean PBL height at 14:00 LT for CONTROL case. The vector is the 10 m surface wind field (unit: m s^{-1}).

respectively. For low-intensity residential areas, the peak ensemble UHI intensity is about 1.2°C–1.3°C at 00:00 LT and then gradually decreases until noon. After sunrise (07:00 LT), UHI intensities for all urban areas decrease quickly and an urban cool island forms during noon (Figure 6a). This urban cool island results from different heat capacities in urban and rural areas, as well as the shading effect in urban areas, especially for commercial/industrial areas where buildings are highest. All of the above characteristics are consistent with the observational study carried out by *Chow* [2004] in Singapore during the same season (before southwest monsoon). While both the current numerical study and observational study by *Chow and Roth* [2006] show that the commercial area has the weakest urban cool island at the noon, an observational study for Hong Kong [*Memon et al.*, 2009] suggests the reverse, i.e., the strongest urban cool island occurs in the area with the highest level of urbanization (defined by building density and development level).

[32] The most notable difference between Figures 6a and 6b is that the latter shows no negative daytime UHI intensity for commercial/industrial areas. This reflects the effect of AH (discussed in section 4.4) and the urban fraction (see Table. 1). A careful examination of Figure 6 reveals that all the UHI intensities calculated by the second method (Figure 6b) are slightly higher than their counterparts by the first method (Figure 6a) by different degrees, with the commercial/industrial area the most and the low-intensity residential area the least. In NoURBAN cases, the urban areas are replaced by rural areas, which increases the vegetation fraction (the sum of urban fraction and vegetation fraction is 1) to 100% from the original 5% for commercial/industrial, 20% for high-intensity residential, and 30% for low-intensity residential areas. This change will decrease the surface temperature in those areas when the meteorological conditions remain unchanged in CONTROL and NoURBAN cases, since more vegetation will introduce more moisture and evaportranspiration. This temperature drop (or urban increment) for the commercial/industrial area is the largest.

[33] Making use of the difference between CONTROL and NoURBAN cases, it is possible to study the spatial variation of UHI. Figure 7 shows the difference in ensemble mean 2 m surface temperature of CONTROL and NoURBAN cases during day (14:00 LT) and night (04:00 LT) time. It is clear that higher temperature differences are associated with urban areas, especially commercial/industrial areas along the southwest (south) of Singapore island during daytime (nighttime). During daytime, this difference is quite small (less than 0.9°C; Figure 7a) since the surface energy balance is mainly dominated by the incoming solar radiation. When solar radiation is not present during night and early morning, the main factors affecting the surface temperature in urban areas are heat storage release, trapped long-wave radiation, and anthropogenic heat. Therefore, the urban areas, commercial/industrial areas in particular, show a much higher temperature difference than other areas, with a maximum of 2.4°C in the west industrial region at 04:00 LT (Figure 7b). The model, however, is likely overestimating the maximum UHI associated with some of the areas classified as commercial/industrial. Since *Quah and Roth* [2012] do not determine AH for industrial areas, their values for commercial land use are used in the model for commercial/industrial category. Most of the industrial areas on the main island of Singapore (e.g., in the southwest) consist of
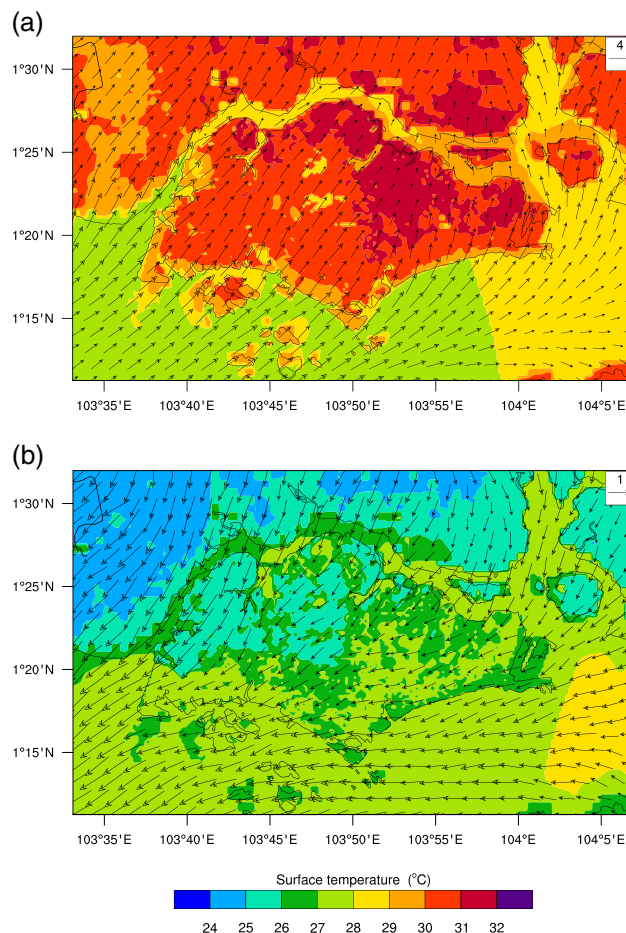

Figure 10. Ensemble mean of the simulated 10 m surface wind field (unit: m s^{-1}) and 2 m surface air temperature at (a) 14:00 LT and (b) 02:00 LT.
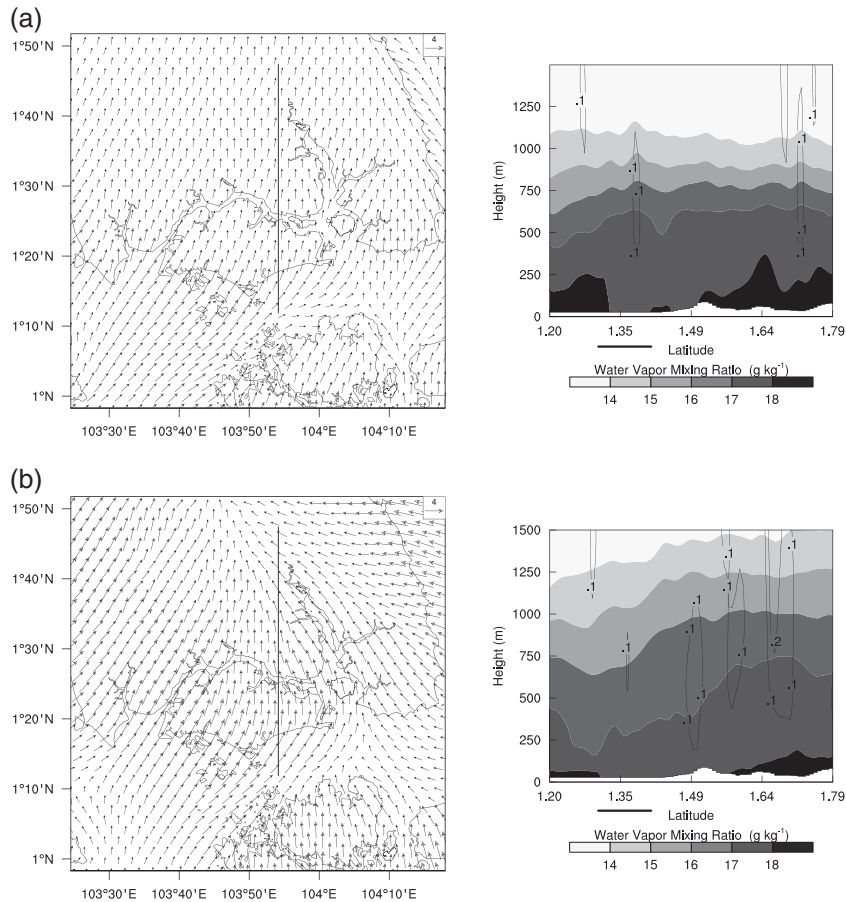
Figure 11. Sea breeze evolution in domain d04 at (a) 11:00 LT and (b) 17:00 LT. (Left) 10 m wind field. The vertical black line indicates the location of the vertical section shown in the right panel. (Right) Vertical cross section showing water vapor mixing ratio (gray scale shades) and vertical velocity at 0.1 m s^{-1} intervals (thin lines, with solid lines for upward motion and dashed lines for downward motion). The horizontal bar shows the extent of Singapore.

flatted factories and low- or medium-rise warehouses, where AH is probably lower than in the densely built commercial areas considered in *Quah and Roth* [2012]. In the numerical study of San Juan, Puerto Rico [*Comarazamy et al.*, 2010], a temperature difference of 2.5°C-3°C between their urban and rural cases was identified, which is similar to the finding in the present study.

4.2. Boundary Layer Development

[34] The PBL height is of fundamental importance for many meteorological applications, especially for air pollution modeling. It is variable in space and time, ranging from hundreds of meters to a few kilometers. Many reports in literature have pointed out that NWP models usually have problems in predicting PBL height [e.g., *Hu et al.*, 2010]. In the MYJ PBL scheme used in the current study, the PBL height is diagnosed as the height where the prognostic TKE reaches a sufficiently small value (0.0005 m^{2}s^{-2}). Figure 8 shows the diurnal variation of the ensemble mean PBL height averaged by land use/land cover types. It is evident that PBL height has a strong diurnal cycle and the land use type has a great impact on PBL height from late afternoon to early morning. As expected, the PBL height commences growth from about 1 h after sunrise (i.e., 08:00

LT), when effective heating of the soil takes place, then stabilizes around noon. The peak PBL height occurs at around 14:00 LT for the three urban land use areas, while at 13:00 LT for rural land use area. During the afternoon to evening, the PBL height decays very quickly, with the fastest rate in rural area until sunset (19:00 LT). In the CONTROL case (Figure 8a), during night and early morning, the three urban land use areas have a rather stable PBL height between 100 and 300 m, while the rural area has a shallow PBL height of 50–100 m. By comparing the CONTROL and NoAH cases (Figures 8a and 8b), it can be seen that AH is the main cause for this difference in nocturnal PBL height for urban and rural areas. If there is no AH, the PBL height for all the land use areas will be almost the same during early morning (Figure 8b). Recently, a similar study by *Bohnenstengel et al.* [2013] for London reported that the AH can maintain a well-mixed boundary layer in winter, which would otherwise be absent without AH.

[35] A noteworthy phenomenon about PBL height in Figure 8 is that, during noon, the PBL height for commercial/industrial areas is lower than those for the other urban and rural land use areas. This can be explained by the sea breezes developed along the coasts during noon (details will be discussed in the next section). The spatial distribution
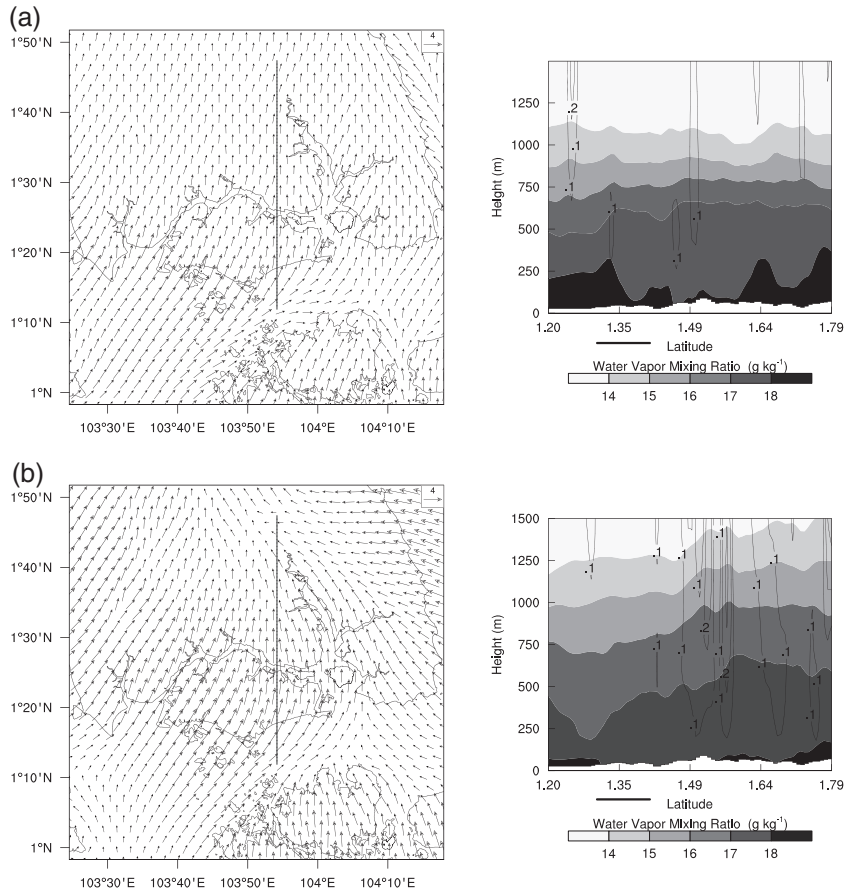
Figure 12. The same as Figure 11 but for NoURBAN cases.

of PBL height at 14:00 LT is depicted in Figure 9, which also shows the sea breeze from southwest. When the sea breeze is developing, the PBL is in the transition from the sea to the land and the PBL height increases with inland distance; a thermal internal boundary layer across the coastline develops, which also suppresses the PBL height [*Sicard et al.*, 2006]. Therefore, the areas along the coastline, most of which are commercial and industrial areas as seen from Figure 2b, show a lower PBL height compared with inland areas (Figure 9).

4.3. Local Circulations

[36] As a coastal city located at the southern tip of Malay Peninsula, Singapore has complex local circulations (sea and land breezes) driven by differential heating between land and sea. These local circulations are important mechanisms for air pollution transport in coastal regions. The sea breeze usually develops when solar irradiation is maximum, i.e., around noon. Figure 10a shows the sea breeze from the southwest toward the Singapore coast at 14:00 LT with a strength of about 4 m s^{-1}. The wind speed reduces in the city area, and the sea breeze flows further inland to the Malay Peninsula. This sea breeze system begins at about 11:00 LT and continues until 17:00 LT. During early morning at 02:00 LT, a northeasterly land breeze system develops, blowing from the Malay Peninsula to the sea (Figure 10b). The land breeze is much weaker (< 1 m s^{-1}) than the sea breeze and does not penetrate far into the sea.

[37] The sea/land breezes shown here are only part of the sea/land breeze systems commonly found in the Malay Peninsula. Due to the complex coastlines and relatively flat terrain in the southern Malay Peninsula, there are often complicated interactions between sea breezes in this area [*Joseph et al.*, 2008]. The sea breeze evolution over the southern Malay Peninsula can be seen from Figure 11 for the domain d04. The wind field plots in the left panel clearly show that the sea breezes onshore from Singapore, the east coast and south coast of Malaysia, meet and converge at different locations. At 11:00 LT, the sea breeze along the east coast of the Malay Peninsula just starts to form and its strength is quite weak (Figure 11a). There are several updrafts induced by convergences (at latitudes of about 1.47° and 1.60°) of different sea breezes from other directions. The strong updrafts of 0.3 m s^{-1} at about 1.35° are induced by the high surface temperature in Singapore urban areas. At 17:00 LT (Figure 11b), the strong sea breeze from the east coast of the Malay Peninsula converges with the sea breeze from the Singapore coast and results in a strong updraft of 0.2 m s^{-1}. The sea breezes from coasts of the Malay Peninsula peak at about 14:00 LT and continue until about 19:00 LT.

[38] To investigate the effect of urban areas in the development of the sea breeze, the same plot as Figure 11 is shown for the NoURBAN case in Figure 12. It should be noted that in the NoURBAN case, only the Singapore urban area has been replaced by rural land use. No urban areas in Malaysia are modified, and this may underestimate the

urban effects in the wider region outside Singapore. The higher surface temperature in urban areas makes the land-sea temperature contrast larger, thus making the strength of the updrafts over the urban area in Singapore (at the latitude of about 1.36°) in the CONTROL case (Figure 11b) stronger than in the NoURBAN case (Figure 12b). Through comparing the mixing ratio contours in Figures 11 and 12, it can be seen that the NoURBAN case has higher moisture than in the CONTROL case over Singapore partially due to the sea breeze confluence.

4.4. Effects of Anthropogenic Heat

[39] Anthropogenic heat is the energy released from human sources such as vehicles, commercial and residential buildings, industry, power plants, and human metabolism [*Quah and Roth*, 2012]. It will affect the urban environment by directly changing the air temperature and indirectly modifying other conditions. In this section, the effects of AH are investigated based on the NoAH case described earlier.

[40] Figure 13a shows the temperature difference between CONTROL and NoAH cases for different land use types. It is evident that AH increases the surface temperature for all land use types by different degrees, with the commercial/industrial areas the most and rural areas the least. The rural area does not have AH, and the temperature increment should be due to the local advection from adjacent urban areas. The diurnal variation shows that AH plays a large role mainly from late afternoon to early morning, when the solar radiation does not dominate the surface energy balance. The only exception is for the commercial/industrial areas, where the temperature increment, exhibiting the similar diurnal cycle to other areas, is high (> 0.5°C) throughout the whole day mainly due to its high absolute value of AH (1 order of magnitude higher than the other two urban categories). For the same reason, a sharp temperature increment is observed for commercial/industrial area at 07:00 LT, when its AH reaches a high level and changes little thereafter until 19:00 LT. No similar phenomenon is observed for the other two urban areas.

[41] The UHI intensity calculated by the first method for the NoAH case further demonstrates the important role of AH (Figure 13b). Relative to the UHI intensity computed for the CONTROL case, the maximum UHI intensity drops by 1.2°C, 0.9°C, and 0.9°C for the three urban areas, respectively. The AH also changes the relative urban cool island intensities of the three urban areas during noon time, making the commercial/industrial area the coolest. This signifies that the positive contribution of AH to the surface temperature in commercial/industrial area overcomes the negative contribution of shading effects and of sea breezes, which makes the commercial/industrial area the hottest urban area during noon in the CONTROL case (see Figure 6a). Without AH, the maximum UHI intensity for the low-intensity residential area appears at 20:00 LT, 1 h after sunset. This reveals that during evening and early morning, AH plays a very important role in the surface energy balance of the low-intensity residential area since this area does not have much heat storage (due to its small building volume) and radiation trapping (due to its low building height).

[42] The spatial patterns of the surface temperature differences between CONTROL and NoAH cases are shown in Figure 14 at differen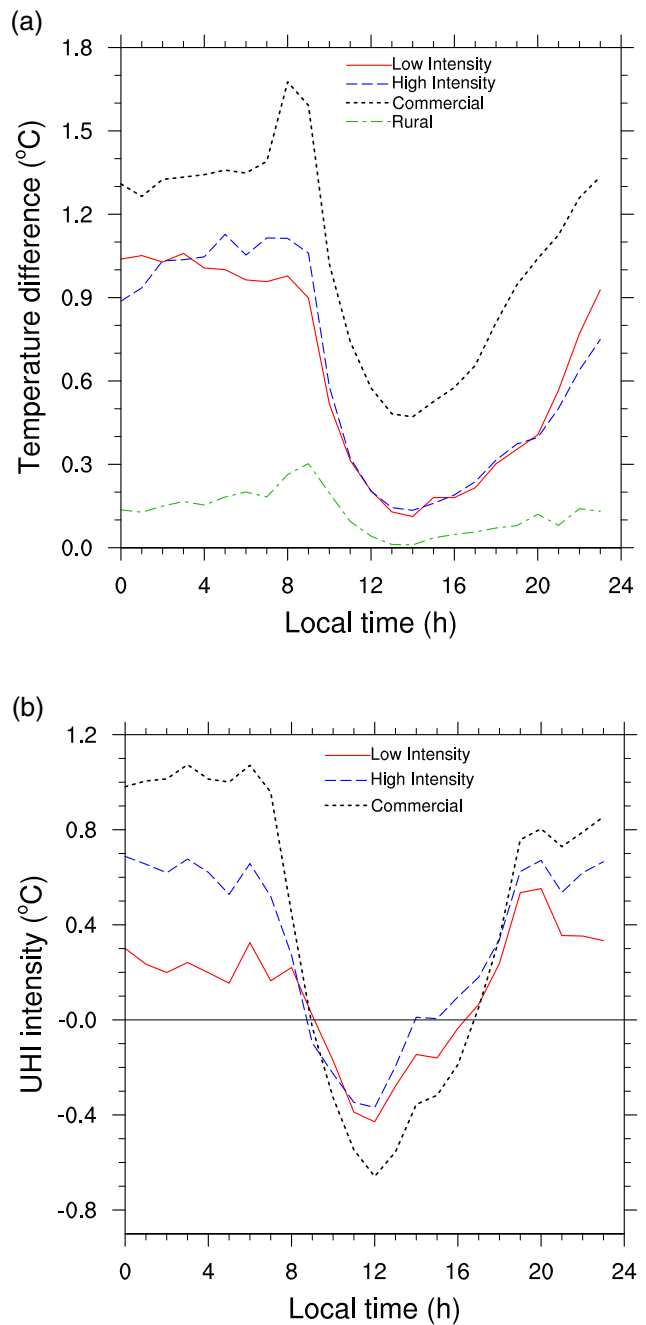t times. The positive temperature differences are associated with urban areas, with the magnitude lower in the afternoon (14:00 LT) and much higher in the early morning (04:00 LT). The maximum temperature differences at both times are observed in the dense industrial region in the western part of Singapore Island. By comparing Figures 7b and 14b, it can be seen that the AH contributes 1.6°C to the maximum UHI intensity of 2.4°C in that region, while other factors (urban morphology and building materials) contribute less. This is consistent with a recent study by *Ryu and Baik* [2012], in which they quantified the relative

(a)

(b)

Figure 13. (a) Diurnal variations of the temperature difference between CONTROL and NoAH cases for different land use types and (b) diurnal variation of the UHI intensity for NoAH cases.
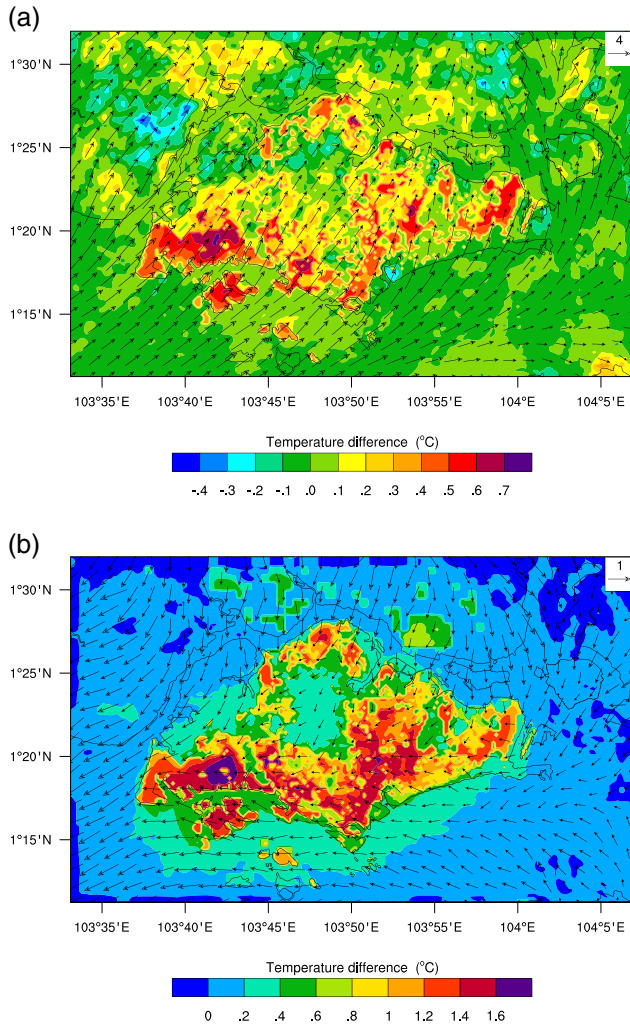
Figure 14. Differences of the ensemble mean 2 m surface temperature between the CONTROL and NoAH cases at (a) 14:00 LT and (b) 04:00 LT. The vector is the 10 m surface wind field of the CONTROL case at the same time (unit: m s^{-1}).

contribution of different causative factors to UHI intensity in a mid-latitude city and concluded that AH contributed the most in the nighttime. It should be noted that, due to the reason described in section 4.1, the AH value for the western industrial areas may be overestimated and thus, the contribution by AH to the maximum UHI intensity is likely overpredicted.

[43] Another factor may also suggest overprediction of UHI intensity in the present study: The AH values used here assume that all of AH is rejected as sensible heat flux into the lower atmosphere. This way, the UHI intensity values reported here present an upper limit of the real value. In reality, some commercial buildings, government buildings and hotels use cooling towers which reject heat from a building by evaporating water that is introduced into the tower and by heating air that flows through the tower. While the simulation of the AH as combined sensible and latent heat fluxes is beyond the scope of the present study, it certainly points to a possible future research direction.

5. Conclusions

[44] The urban environment in a tropical city, Singapore, has been investigated using the Weather Research and Forecasting (WRF) model coupled to a single-layer urban canopy model (UCM) using an ensemble approach. The coupled system was first evaluated against surface observations from a sensor network and energy balance measurements from a flux tower. It was shown that the model can simulate well the temperature distribution and surface energy balance characteristics but not the specific humidity in Singapore across different land use types. Normalized error variance diagnostics show that most of the error comes from disagreement in phase of the modeled patterns while agreement in the amplitude is excellent.

[45] Numerical simulations were then performed at a high spatial resolution of 300 m for an ensemble of low advection, high CAPE, intermonsoon cases for Singapore in order to make local effects dominate. The diurnal cycle and spatial distribution of the ensemble mean urban heat island (UHI) intensity were studied. The modeled UHI intensity peaked in early morning and kept constant during late night and early morning, and it could reach 2.4°C during early morning in the intense industrial region in western Singapore. Anthropogenic heat (AH) played an important role in UHI intensity, contributing 1.6°C to the maximum UHI intensity and 1.2°C to the mean UHI intensity in the commercial/industrial areas. The effect of different urban land use types was most pronounced during the night and least visible during the noon.

[46] The study of planetary boundary layer (PBL) development showed that the PBL height had a strong diurnal cycle and the land use type only affected PBL height from late afternoon to early morning. AH was primarily responsible for the 100–300 m high nocturnal PBL. The spatial distribution of PBL height suggested that the sea breeze which developed during noon reduced the PBL height in the commercial/industrial areas, the majority of which are located adjacent to the coastline.

[47] Local circulations (sea and land breezes) developed during daytime and nighttime, respectively, with the former usually stronger than the latter. Some complicated interactions between onshore sea breezes from different coastlines of the Malay Peninsula were observed, as reported by *Joseph et al.* [2008]. It has been demonstrated that the sea surface temperature and soil moisture are important in determining local circulations in coastal areas [*Chen et al.*, 2011b]. A similar sensitivity study of these parameters is needed in the future to identify their roles in the sea/land breezes in Singapore and the Malay Peninsula.

[48] Due to the limitation of the three-class UCM used in this study, it is not possible to identify the intra-urban variability of local characteristics (e.g., sky view factor and street aspect ratio) and hence, the intra-urban variation of local wind and thermal environment within the same urban land use/land cover type. With the help of a more detailed urban morphology database, more sophisticated UCMs may achieve this goal at the expense of more computational resources.

References

Arnfield, A. J. (2003), Two decades of urban climate research: A review of turbulence, exchanges of energy and water, and the urban heat island, *Int. J. Climatol.*, *23*(1), 1–26.

Baklanov, A., J. Ching, C. Grimmond, and A. Martilli (2009), Model urbanization strategies: Summaries, recommendations and requirements, in *Urbanization of Meteorological and Air Quality Models*, edited by A. Baklanov et al., chap. 15, pp. 151–162, Springer-Verlag, Berlin Heidelberg.

Bohnenstengel, S. I., S. Evans, P. A. Clark, and S. Belcher (2011), Simulations of the London urban heat island, *Q. J. R. Meteorolog. Soc.*, *137B*, 1625–1640.

Bohnenstengel, S. I., I. Hamilton, M. Davies, and S. E. Belcher (2013), Impact of anthropogenic emissions on London's temperatures, *Q. J. R. Meteorolog. Soc.*, doi:10.1002/qj.2144.

Chemel, C., and R. S. Sokhi (2012), Response of London's urban heat island to a marine air intrusion in an easterly wind regime, *Bound. Lay. Meteorol.*, *144*(1), 65–81.

Chen, F., and J. Dudhia (2001), Coupling an advanced land-surface–hydrology model with the Penn State/NCAR MM5 modeling system. Part I: Model implementation and sensitivity, *Mon. Wea. Rev.*, *129*, 569–585.

Chen, F., et al. (2011a), The integrated WRF/urban modelling system: Development, evaluation, and applications to urban environmental problems, *Int. J. Climatol.*, *31*(2), 273–288.

Chen, F., S. Miao, M. Tewari, J.-W. Bao, and H. Kusaka (2011b), A numerical study of interactions between surface forcing and sea breeze circulations and their effects on stagnation in the greater Houston area, *J. Geophys. Res.*, *116*, D12105, doi:10.1029/2010JD015533.

Chia, L. S., and S. F. Foong (1991), Climate and weather, in *The Biophysical Environment of Singapore*, edited by L. S. Chia, A. Rahman, and D. B. H. Tay, pp. 13–49, Singapore University Press and the Geography Teachers' Association of Singapore, Singapore.

Ching, J., et al. (2009), National Urban Database and Access Portal Tool (NUDAPT), *Bull. Am. Meteorol. Soc.*, *90*, 1157–1168.

Chow, W. T. L. (2004), The temporal dynamics of the urban heat island of Singapore, Master thesis, National University of Singapore, 177 pp.

Chow, W. T. L., and M. Roth (2006), Temporal dynamics of the urban heat island of Singapore, *Int. J. Climatol.*, *26*(15), 2243–2260.

Comarazamy, D. E., J. E. González, J. C. Luvall, D. L. Rickman, and P. J. Mulero (2010), A land-atmospheric interaction study in the coastal tropical city of San Juan, Puerto Rico, *Earth Interact.*, *14*, 1–24, doi:10.1175/2010EI309.1.

Cox, R., B. L. Bauer, and T. Smith (1998), Mesoscale model intercomparison, *Bull. Am. Meteorol. Soc.*, *79*, 265–283.

Essenwanger, O. M. (2001), Classification of climates, *World Survey of Climatology 1C, General Climatology*, p. 102, Elsevier, Amsterdam.

González, J. E., et al. (2005), Urban heat islands developing in coastal tropical cities, *Eos Trans. AGU*, *86*, 397–401, doi:10.1029/2005EO420001.

Grimmond, C. S. B. (2006), Progress in measuring and observing the urban atmosphere, *Theor. Appl. Climatol.*, *84*, 3–22.

Grimmond, C. S. B., and T. R. Oke (1999), Heat storage in urban areas: Local-scale observations and evaluation of a simple model, *J. Appl. Meteorol. Climatol.*, *38*, 922–940.

Grimmond, C. S. B., et al. (2010), The international urban energy balance models comparison project: First results from Phase 1, *J. Appl. Meteorol. Climatol.*, *49*, 1268–1292.

Grimmond, C. S. B., et al. (2011), Initial results from Phase 2 of the international urban energy balance model comparison, *Int. J. Climatol.*, *31*, 244–272.

Hawkins, T. W., A. J. Brazel, W. L. Stefanov, W. Bigler, and E. M. Saffell (2004), The role of rural variability in urban heat island determination for Phoenix, Arizona, *J. Appl. Meteorol.*, *43*(3), 476–486.

Heisler, G. M., and A. J. Brazel (2010), The urban physical environment: Temperature and urban heat islands, in *Urban ecosystem ecology*, edited by J. Aitkenhead-Peterson and A. Volder, pp. 29–56, American Society of Agronomy, Madison, Wisc.

Holt, T., and J. Pullen (2007), Urban canopy modeling of the New York City metropolitan area: A comparison and validation of single- and multilayer parameterizations, *Mon. Wea. Rev.*, *135*, 1906–1930.

Holt, T., J. Pullen, and C. H. Bishop (2009), Urban and ocean ensembles for improved meteorological and dispersion modelling of the coastal zone, *Tellus*, *61A*(2), 232–249.

Hu, X.-M., J. W. Nielsen-Gammon, and F. Zhang (2010), Evaluation of three planetary boundary layer schemes in the WRF model, *J. Appl. Meteorol. Climatol.*, *49*(9), 1831–1844.

Hunt, J. C., Y. V. Timoshkina, S. I. Bohnenstengel, and S. Belcher (2013), Implications of climate change for expanding cities worldwide, *Proceedings of the ICE - Urban Design and Planning*, *166*, 241–254, doi:10.1680/udap.10.00062.

Ichinose, T., K. Shimodozono, and K. Hanaki (1999), Impact of anthropogenic heat on urban climate in Tokyo, *Atmos. Environ.*, *33*, 3897–3909.

Inamura, T., T. Izumi, and H. Matsuyama (2011), Diagnostic study of the effects of a large city on heavy rainfall as revealed by an ensemble simulation: A case study of central Tokyo, Japan, *J. Appl. Meteorol. Climatol.*, *50*, 713–728.

Jauregui, E. (1997), Heat island development in Mexico City, *Atmos. Environ.*, *31*, 3821–3831.

Joseph, B., B. C. Bhatt, T. Y. Koh, and S. Chen (2008), Sea breeze simulation over the Malay Peninsula in an intermonsoon period, *J. Geophys. Res.*, *113*, D20122, doi:10.1029/2008JD010319.

Koh, T.-Y., and J. S. Ng (2009), Improved diagnostics for NWP verification in the tropics, *J. Geophys. Res.*, *114*, D12102, doi:10.1029/2008JD011179.

Koh, T.-Y., S. Wang, and B. C. Bhatt (2012), A diagnostic suite to assess NWP performance, *J. Geophys. Res.*, *117*, D13109, doi:10.1029/2011JD017103.

Kusaka, H., and F. Kimura (2004), Coupling a single-layer urban canopy model with a simple atmospheric model: Impact on urban heat island simulation for an idealized case, *J. Meteorol. Soc. Jpn.*, *82*, 67–80.

Kusaka, H., H. Kondo, Y. Kikegawa, and F. Kimura (2001), A simple single-layer urban canopy model for atmospheric models: Comparison with multi-layer and slab models, *Boundary. Layer. Meteorol.*, *101*, 329–358.

Kusaka, H., F. Kimura, K. Nawata, T. Hanyu, and Y. Miya (2009), The chink in the armor: Questioning the reliability of conventional sensitivity experiments in determining urban effects on precipitation patterns, paper presented at Seventh International Conference on Urban Climate, Yokohama, Japan.

Landsberg, H. E. (1981), *The Urban Climate, International Geophysics Series*, vol. 28, Academic Press, New York.

Lee, S.-H., S.-W. Kim, W. M. Angevine, L. Bianco, S. A. McKeen, C. J. Senff, M. Trainer, S. C. Tucker, and R. J. Zamora (2011), Evaluation of urban surface parameterizations in the WRF model using measurements during the Texas Air Quality Study 2006 field campaign, *Atmos. Chem. Phys.*, *11*, 2127–2143, doi:10.5194/acp-11-2127-2011.

Li, R. M. (2013), Spatio-temporal dynamics of the urban heat island in Singapore, Master thesis, National University of Singapore. 163 pp.

Lin, C.-Y., F. Chen, J. Huang, Y. A. Liou, W. C. Chen, W. N. Chen, and S. C. Liu (2008), Urban heat island effect and its impact on boundary layer development and land–sea circulation over northern Taiwan, *Atmos. Environ.*, *42*, 5639–5649.

Martilli, A., A. Clappier, and M. W. Rotach (2002), An urban surface exchange parameterization for mesoscale models, *Bound. Lay. Meteorol.*, *104*, 261–304.

Martin, C., L. Stabler, and A. Brazel (2000), Summer and winter patterns of air temperature and humidity under calm conditions in relation to urban land use, in *3rd Symposium on the Urban Environment*, pp. 197–198, American Meteorological Society, Davis, CA, USA.

Memon, R. A., D. Y. Leung, and C.-H. Liu (2009), An investigation of urban heat island intensity (UHII) as an indicator of urban heating, *Atmos. Res.*, *94*, 491–500.

Miao, S., F. Chen, M. LeMone, M. Tewari, Q. Li, and Y. Wang (2009), An observational and modeling study of characteristics of urban heat island and boundary layer structures in Beijing, *J. Appl. Meteorol. Climatol.*, *48*, 484–501.

Murphy, D. J., M. H. Hall, C. A. S. Hall, G. M. Heisler, S. V. Stehman, and C. Anselmi-Molina (2011), The relation between land cover and the urban heat island in northeastern Puerto Rico, *Int. J. Climatol.*, *31*, 1222–1239, doi:10.1002/joc.2145.

Oke, T. R. (1976), The distinction between canopy and boundary-layer urban heat islands, *Atmosphere*, *14*(4), 268–277.

Oke, T. R. (1982), The energetic basis of the urban heat island, *Quart. J. Roy. Meteorol. Soc.*, *108*, 1–24.

Onset Computer Corporation (2007), HOBO Pro v2. Doc #10694-F, MAN-U23.

Pigeon, G., A. Lemonsu, N. Long, J. Barrié, V. Masson, and P. Durand (2006), Urban thermodynamic island in a coastal city analysed from an optimized surface network, *Bound. Lay. Meteorol.*, *120*, 315–351.

Quah, A. K., and M. Roth (2012), Diurnal and weekly variation of anthropogenic heat emissions in a tropical city, Singapore, *Atmos. Environ.*, *46*, 92–103.

Roth, M. (2007), Review of urban climate research in (sub)tropical regions, *Int. J. Climatol.*, *27*, 1859–1873.

Roth, M., and W. T. L. Chow (2012), A historical review and assessment of urban heat island research in Singapore, *Singapore J. Tropical Geog.*, *33*, 381–397.

Ryu, Y.-H., and J.-J. Baik (2012), Quantitative analysis of factors contributing to urban heat island intensity, *J. Appl. Meteorol. Climatol.*, *51*, 842–854.

Salamanca, F., A. Martilli, M. Tewari, and F. Chen (2011), A study of the urban boundary layer using different urban parameterizations and high-resolution urban canopy parameters with WRF, *J. Appl. Meteorol. Climatol.*, *50*, 1107–1128.

Salamanca, F., A. Martilli, and C. Yagüe (2012), A numerical study of the Urban Heat Island over Madrid during the DESIREX (2008) campaign with WRF and an evaluation of simple mitigation strategies, *Int. J. Climatol.*, *32*, 2372–2386, doi:10.1002/joc.3398.

Schlünzen, K. H., and J. J. Katzfey (2003), Relevance of sub-grid-scale land-use effects for mesoscale models, *Tellus*, *55A*, 232–246.

Sicard, M., C. Pérez, F. Rocadenbosch, J. M. Baldasano, and D. García-Vizcaino (2006), Mixed-layer depth determination in the Barcelona coastal area from regular lidar measurements: Methods, results and limitations, *Bound. Lay. Meteorol.*, *119*, 135–157.

Skamarock, W. C., J. B. Klemp, J. Dudhia, D. O. Gill, D. M. Barker, M. G. Duda, X.-Y. Huang, W. Wang, and J. G. Powers, (2008), A description of the Advanced Research WRF version 3, *Technical note TN-475+STR*, 113 pp., NCAR.

Souch, C., and S. Grimmond (2006), Applied climatology: Urban climate, *Prog. Phys. Geog.*, *30*, 270–279.

Willmott, C. J. (1981), On the validation of models, *Phys. Geog.*, *2*(2), 184–194.

Yow, D. M. (2007), Urban heat islands: Observations, impacts, and adaptation, *Geog. Comp.*, *1*, 1227–1251.

Zhou, L., R. E. Dickinson, Y. Tian, J. Fang, Q. Li, R. K. Kaufmann, C. J. Tucker, and R. B. Myneni (2004), Evidence for a significant urbanization effect on climate in China, *Proc. Nat. Acad. Sci. USA*, *101*, 9540–9544.